CCD Video Observation of Microgravity Crystallization of Lysozyme and Correlation with Accelerometer Data

E. H. SNELL,[a]† T. J. BOGGON,[a] J. R. HELLIWELL,[a]* M. E. MOSKOWITZ[b] AND A. NADARAJAH[c]

[a]*Chemistry Department, University of Manchester, Oxford Road, Manchester M13 9PL, England,* [b]*Tal-Cut Company, PIMS Group, NASA Lewis Research Center, 21000 Brookpark Road, Mailstop 500-216, Cleveland, OH 44135, USA, and* [c]*Macromolecular Engineering Laboratory, Department of Chemical Engineering, 3056 Nitschke Hall, Toledo, Ohio 43606-3390, USA. E-mail: john.helliwell@man.ac.uk*

Abstract

Lysozyme has been crystallized using the ESA Advanced Protein Crystallization Facility onboard the NASA Space Shuttle Orbiter during the IML-2 mission. CCD video monitoring was used to follow the crystallization process and evaluate the growth rate. During the mission some tetragonal crystals were observed moving over distances of up to 200 μm. This was correlated with microgravity disturbances caused by firings of vernier jets on the Orbiter. Growth-rate measurement of a stationary crystal (which had nucleated on the growth reactor wall) showed spurts and lulls correlated with an onboard activity: astronaut exercise. The stepped growth rates may be responsible for the residual mosaic block structure seen in crystal mosaicity and topography measurements.

1. Introduction

Microgravity as a growth environment reduces convection buoyancy effects and sedimentation and has produced the most perfect protein crystals yet (Snell *et al.*, 1995). The European Space Agency (ESA) have developed the Advanced Protein Crystallization Facility (APCF) (Snyder, Fuhrmann & Walter, 1991; Bosch, Lautenschlager, Potthast & Stapelmann, 1992) for microgravity crystallization. Three crystallization methods are supported, dialysis, liquid–liquid (free-interface) diffusion and vapour diffusion. Chicken egg-white lysozyme is used as a standard test material to investigate protein crystal growth and nucleation (*e.g.* Ataka & Asai, 1988; Durbin & Feher, 1986; Howard, Twigg, Baird & Meehan, 1988; Pusey, Witherow & Naumann, 1988). This work used the dialysis method for microgravity crystallization experiments with lysozyme. This report focuses on the information provided by CCD video observation during the growth process and correlation with data from the Space Acceleration Measurement System (SAMS).

---

† Current address: NASA, Laboratory for Structural Biology, Code ES76, Building 4464, MSFC, Huntsville, AL 35812, USA.

2. Experimental

2.1. *Equipment*

Within the APCF 48 crystallization experiments are accommodated at constant temperature, in this case 293±0.1 K. Two groups of six reactors in the facility are monitored with a black and white CCD video camera (582 lines with 500 pixels per line) using wide (8.5 × 6.4 mm) or narrow field of view (4.9 × 3.7 mm). Illumination is provided by an 850 nm wavelength polarized light-emitting diode (LED) and images are digitized and stored on magnetic tape for later analysis on Earth. The dialysis reactor, described elsewhere (Bosch *et al.*, 1992; Snell, Helliwell, Boggon, Lautenschlager & Potthast, 1996) consists of three chambers; one containing protein and buffer solution, one for buffer and one containing a salt solution. The salt solution is brought into contact with the protein and buffer by a 90° rotation of a plug which also contains a salt solution volume. Crystal nucleation and growth occur as the salt diffuses into the protein volume. The reactor is deactivated by a further 90° rotation of the plug.

The microgravity and vibration environment of the Orbiter is measured by the space acceleration measurement system (SAMS). The SAMS unit consists of three remote triaxial (acceleration) sensor heads (TSH) and a control and data recording unit. Details of the SAMS system are given elsewhere (DeLombard, Finley & Baugher, 1992; DeLombard & Finley, 1991). The raw data collected by SAMS is processed to compensate for temperature and gain-related errors of bias, scale factor and axis misalignment within the sensor heads. For this work triaxial sensor head *A* was recorded at 50 samples per second and triaxial sensor head *C* at 500 samples per second. Prior to data digitization, low-pass filters of 10 and 100 Hz were applied to the data from sensor heads *A* and *C*, respectively, to prevent signal aliasing.

A number of data-analysis techniques may be used with the SAMS data. Here a time-domain analysis was performed by taking the root mean square (RMS) of the data from the three axes followed by computing the root

sum of squares (RSS). In this fashion the data is combined into a single vector magnitude quantity. A plot of this data gives a measure of the oscillatory content in the data. SAMS data may also be analysed in the frequency domain by producing a spectrogram plot [showing power spectral density (PSD) intensity *versus* time]. In this case spectrograms have been produced by computing PSD's from successive 16.384 s periods, assigning a colour to the base 10 logarithm of the PSD intensity, and then stacking these successive strips from left to right, so that time increases on the x axis of the plot. This technique allows a chart of the acceleration environment to be created.

2.2. Crystallization

A solution of 21 mg of lysozyme [3× crystallized, dialysed and lyophilized powder of chicken egg-white lysozyme supplied by Sigma batch number (Lot) 111 H7010] dissolved in 250 µl 0.4 M acetate buffer (pH 4.7) was used to fill the protein chamber (188 µl). The salt chambers (541 µl) were filled with 1.26 M NaCl and the buffer chamber (59 µl) with 0.04 M acetate buffer (pH 4.7). Sodium azide was also added to the protein and buffer solution as an antifungal agent [1.92 × 10^{-3} mg (188 µl)$^{-1}$]. Addition of antifungal agents prevents aging effects in the solution (Chayen, Radcliffe & Blow, 1993) and reduces nucleation which would otherwise produce a large number of smaller crystals rather than the few larger crystals which were observed. Identical material and reactors were used in ground controls. The APCF was held at 293±0.1 K. The ground controls were held within a polystyrene box in a temperature-controlled room at 293±1 K in a vertical orientation with the protein chamber uppermost, *i.e.* the least turbulent orientation (Snell *et al.*, 1996).

Photographs were taken of the protein chamber before the reactor was inserted into the APCF facility and handed over to NASA for payload integration. There was no sign of crystal formation before the mission. The APCF was launched (July 8th, 1994) on the NASA Space Shuttle International Microgravity Laboratory-2 (IML-2) STS-65 mission in the mid-deck locker of the Orbiter. Nucleation and growth took place in microgravity over a period of approximately 300 h (12.5 d).

The APCF was activated 2 h and 30 min into the mission, a mission elapsed time (MET) of 0 d 2 h and 30 min (expressed as MET 000/02:30). The APCF internal clock was started at this point consequently APCF generated timings lag MET by 2 h and 30 min. CCD monitoring of the crystals, using the narrow field-of-view optics took place every 8 h and 40 min. These monitoring periods entailed the capture of nine images taken from successive focal points throughout the reactor using a 5 min interval between images. The final image (the 36th measurement group) was recorded at 296.32 h, prior to reactor deactivation. After landing, the APCF

was removed from the Orbiter mid-deck and photographs of the reactor taken (Fig. 1).

3. Results and analysis

3.1. Crystals

Exceptionally nice tetragonal crystals were produced in terms of morphology and size, with an average dimension of 1.8 mm with a maximum of 2.5 mm (Fig. 1b). The ground control crystals were smaller, 0.6 mm on average, 0.8 mm at maximum. Sedimentation and clumping were not in evidence for the microgravity-grown tetragonal lysozyme crystals but was observed in the ground controls. Of note within the flight reactor (but not in the ground control case) was the presence of a minority of orthorhombic crystals as well as the more numerous tetragonal crystals. For the orthorhombic form two distinct sub-groups were observed; a small number of single 'needle'-shaped crystals (up to a length of 2.1 mm) extruding from the surfaces of particular tetragonal crystals, (Fig. 1c) and clumps of orthorhombic crystals (with a maximum length approximately 1.0 mm) (Fig. 1d). Both orthorhombic and tetragonal forms were confirmed by X-ray diffraction data collections at the ESRF.

3.2. Crystal motion

CCD video monitoring showed that the first (tetragonal) crystals began to appear in images recorded at 36 h and 50 min after activation of the reactor. Unfortunately, in none of the CCD images did we see formation of orthorhombic crystals within the (restricted) field of view. The CCD images (at different focal points during the monitoring period) between the times of 36 h and 50 min and 37 h and 30 min show motion of a tetragonal crystal. Additionally, between the times of 45 h 31 min and 46 h and 8 min motion of two other crystals was observed. This motion is plotted in Fig. 2.

An explanation of this motion is that crystals which grow in solution eventually become of sufficient size in the residual gravitational field to move through the fluid with the Stokes settling velocity (Long *et al.*, 1994). The instantaneous distance travelled by the crystal can be calculated from,

$$l = \frac{2}{9} \frac{R^2 g(\rho_c - \rho_s)t}{\mu}, \qquad (1)$$

where l is the distance moved in the time t, μ is the mother liquor viscosity, ρ_c is the crystal density, ρ_s the mother liquor density, R is the radius of the crystal and g is the residual acceleration on the crystal. This relationship is approximate because it makes several assumptions *i.e.* the crystal has reached terminal velocity, its shape is approximated to a sphere, only a single averaged impulse is considered and no allowance for growth kinetics

during the period of the observation is made. It does, however, allow an estimation of the minimum force acting on the crystal over the time span of the images.

Pusey & Naumann (1986) give $\rho_c = 1.45$ g cm^{-3}, $\rho_s = 1.00$ g cm^{-3} and $\mu = 1.45 \times 10^{-2}$ g cm^{-1} s^{-1}. For the three crystals in which movement is seen, t is known and R and l can be measured (Table 1). If the force acting on the crystals is purely residual acceleration then, the acceleration must be at least 1.9×10^{-4}, 1.4×10^{-5} and 3.3×10^{-5} m s^{-2} for crystals 1 to 3 respectively (19.4, 1.4 and 3.4 μg) in order to produce the movements which were measured. Motion of crystals 2 and 3 were recorded at the same time, although different required values of acceleration were calculated at this instant. This analysis requires an accurate measurement of the volume of the crystal so that the effective radius can be calculated. It is

difficult to accurately measure this volume when only the (101) faces are visible or the crystal (110) face is not parallel to the camera, as seems to be the case for crystal 3.

For crystal motion seen between 36 h and 50 min (MET 001/15:20) and 37 h and 30 min (MET 001/16:01) it can be seen (Fig. 3a) that there are a series of accelerations of greater than 1.37×10^{-5}g, where g is equal to 9.81 m s^{-2}. These start at MET 001/15:00 and last until MET 001/16:00. The RSS value of these accelerations peaks at just under 8×10^{-4}g at MET 001/15:45. In contrast, the crystal motion seen between 45 h 31 min (MET 002/00:01) and 46 h 3 min (002/00:32) shows lower acceleration (Fig. 3b). However, during the period MET 001/22:00 to 002/00:00 acceleration activity is seen between the hours of 22:20 and 23:30 (Fig. 3c).
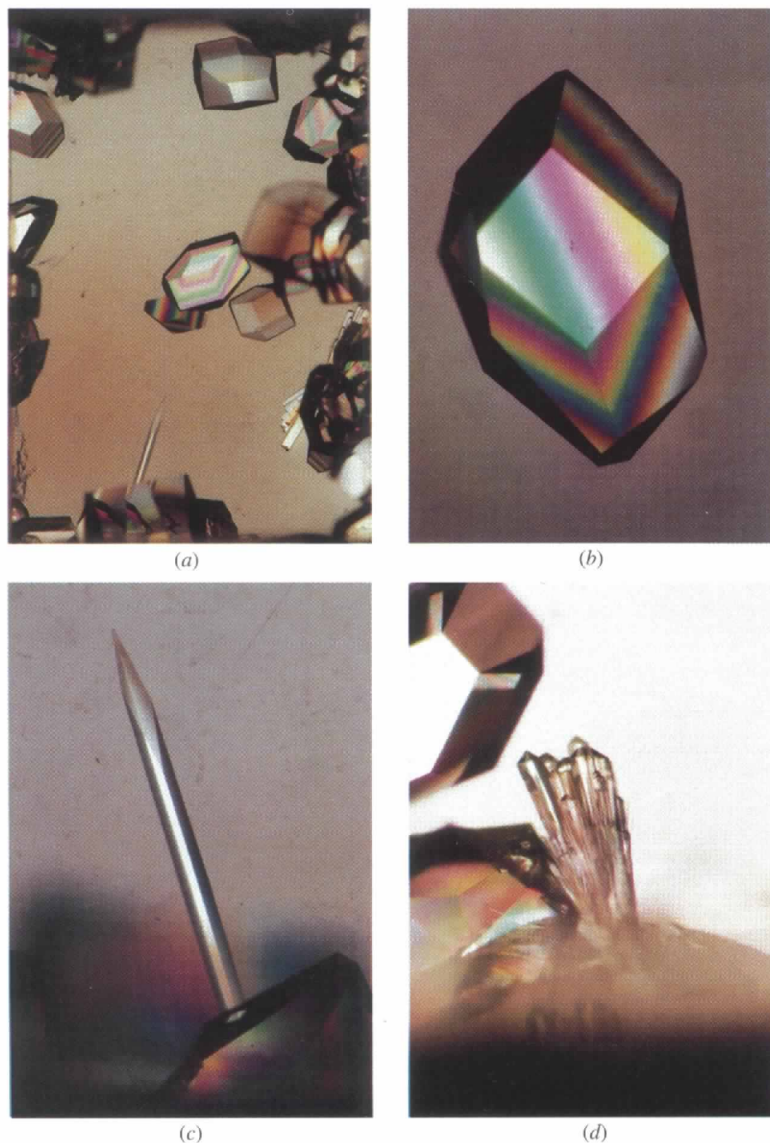

(a)

(b)

(c)

(d)

Fig. 1. Lysozyme crystals produced in microgravity (a) showing the whole protein chamber (for scale the width of the chamber is 5.0 mm). (b) Close up of a typical tetragonal crystal (2.5 mm for the longest dimension). (c) A single needle-shaped orthorhombic lysozyme crystal (length 2.1 mm) growing 'out of' the surface of a tetragonal crystal. (d) Clumps of orthorhombic crystals.

Table 1. *Distance covered during time and approximate radius of the crystals seen in Fig. 2*

For definition of symbols see equation (1).

	l (μm)	t (s)	R (μm)
Crystal 1	377	2419.2	108
Crystal 2	530	2185.2	511
Crystal 3	537	2185.2	274

These accelerations were caused by firings of the Vernier Reaction Control System (VRCS) which is used to control the Orbiter attitude.

3.3. Crystal growth

The CCD camera images show a good example of the microgravity growth of the (110) face of a tetragonal lysozyme crystal (Fig. 4). This crystal was stationary throughout its growth, probably having nucleated on the reactor volume wall.

Plotting the growth rate (Durbin & Feher, 1986) calculated from the difference in half width measured on the (110) face over difference in time, an initial peak of growth rate is followed by a decline (Fig. 5). The growth rate continues its decline until 97 h and 29 min (MET 004/03:59) where it becomes constant, then peaks before the 114 h 46 min observation (MET 004/21:16). During this period, a series of prolonged acceleration impulses, or g-jitter, greater than 500 μg were observed, the worst case is shown in Fig. 6(a). This period of time corresponds to crew exercise activities onboard the Orbiter which took place during the MET 004/18:00 to 004/18:35 and 004/18:45 to 004/19:15 periods.
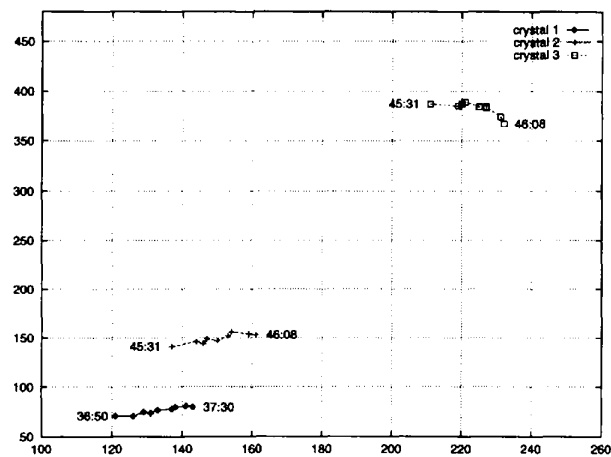

Fig. 2. Plot of protein crystal motion seen in the crystallization reactor (based on the CCD video frames, examples of which are shown in Fig. 4). The units are pixels, where one pixel has a size of 15 × 13 μm (vertical × horizontal). The start and end times of the frame sampling period are given (in h:min after reactor initiation). The timing started on activation of the APCF, 2 h and 30 min into the mission (mission elapsed time 02:30).
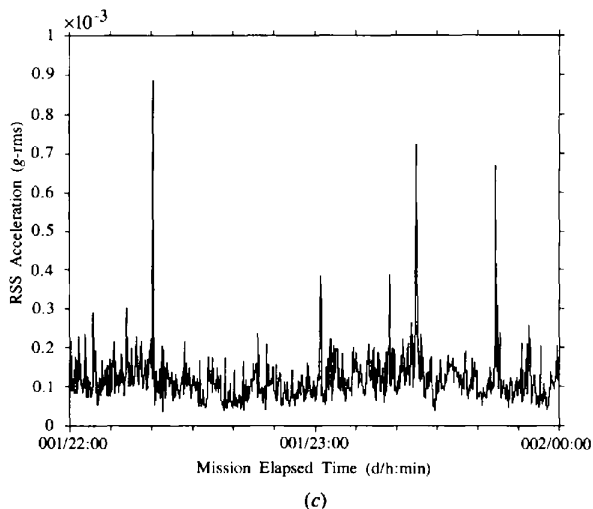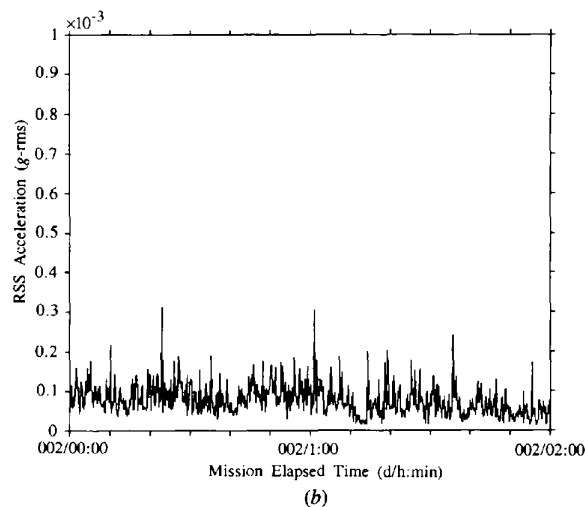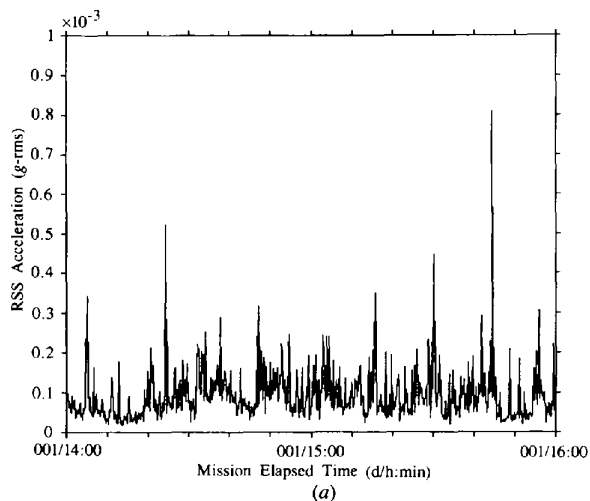

Fig. 3. SAMS plots for the time periods of (a) MET 001/14:00 to 001/16:00 showing acceleration produced by firings of the Vernier Reaction Control System (VRCS) for attitude control of the Orbiter (b) MET 002/00:00–002/02:00 with no VRCS firing and (c) MET 001/22:00–001/24:00 again showing VRCS firing.

Thereafter, growth declines and ceases (Fig. 5) until 140 h, 45 min (MET 005/23:15) after which point another growth spurt is seen. There is a large g-jitter occurring at MET 006/06:10 to 06:40 that approaches 1000 µg at times (*i.e.* milli-g!), Fig. 6(*b*). These accelerations were the result of crew ergometer (a bicycle-type device) exercise which took place on the flight deck. Thereafter, the growth ceases after 158 h 2 min until peaking again at 201 h 19 min (MET 008/ 11:49). Crew exercise occurring at MET 007/06:05 to 007/06:40, 007/07:45 to 007/08:15, 008/04:25 to 008/ 04:55, 008/05:20 to 008/05:50 and 008/06:40 to 008/ 07:10. Again, peaks in the g-jitter are seen during the period just before and during the peak in growth rate.

(*a*) 36:54 h (MET 001/15:24)

(*b*) 45:34 h (MET 002/00:04)

(*c*) 62:52 h (MET 002/17:22)
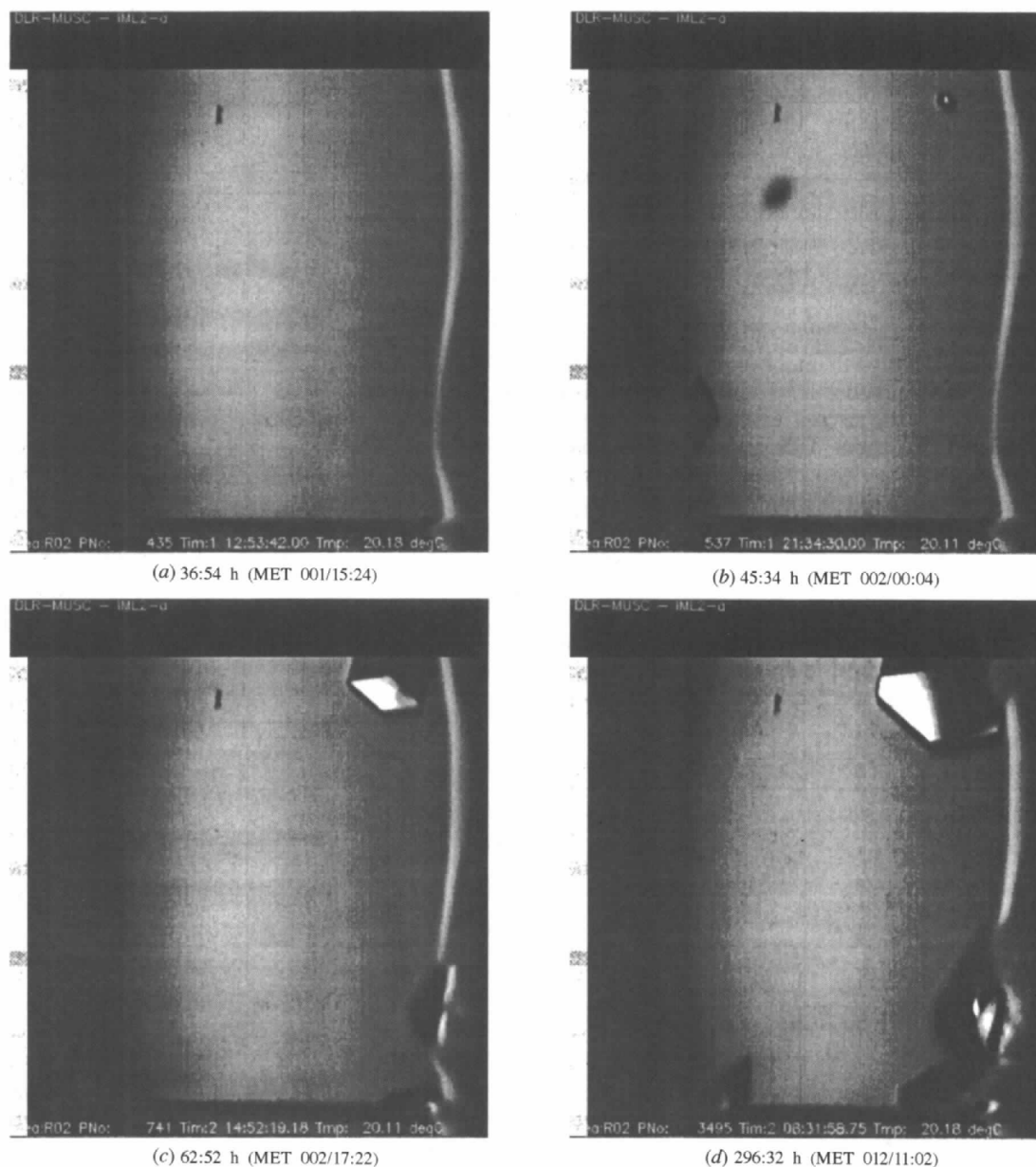
(*d*) 296:32 h (MET 012/11:02)

Fig. 4. Video images of a single, microgravity grown, tetragonal lysozyme crystal (top right of each image), clearly showing the 110 face, at times of (*a*) 36:54 h, (*b*) 45:34 h, (*c*) 62:52 h, and (*d*) 296:32 h (near the end of the mission *i.e.* prior to descent which took place at MET 014/ 15:55). The timings here are APCF times which was activated 2 h 30 mins into the mission (MET 000/02:30). Obviously other time frames are available but not shown here. The timing numbers displayed on each frame relate to the activation of the APCF. Note also the temperature stability of the APCF if monitored from the number in the bottom right of each frame. See also the full video sequence of the crystal growth at http://www.iucr.ac.uk/iucr-top/journals/acta/d/1997/5306/gr0718/.

The *Tiegelfreies Elektromagnetisches Prozessieren Unter Schwerelosigkeit* TEMPUS (Electromagnetic Containerless Processing Facility) water pump was operated at times illustrated in Fig. 5. This facility produces a strong 80 Hz g-jitter due to operation of a water pump within it running at 4800 rev min^{-1}. Fig. 7 shows a spectrogram taken at the start of the TEMPUS water pump operation showing a 4400 µg jitter in the 80 Hz range. Also during this period crew exercise took place on the flight deck using the ergometer. Although this exercise equipment is vibration isolated from the Orbiter acceleration its use is still noticeable in the spectrogram (Fig. 7) from MET 006/06:06 to 006/06:36. The normal frequency for this exercise activity is 2.5 Hz with harmonics, and a 1.25 Hz signal consistent with the crew members shoulders swinging from side to side. Typical individual crew exercise time is 20–35 min.

4. Discussion

4.1. Growth rate and g-jitter incidents

Analyses of crystal growth rates have indicated that the local protein concentration in a growth solution is depleted only when the crystal exceeds a critical size (Pusey, Snyder & Naumann, 1986; Pusey & Naumann, 1986; Grant & Saville, 1991). For tetragonal lysozyme the critical size is around 0.1 mm. When this size is exceeded, concentration gradients develop around the growing crystal and the protein in solution eventually gets depleted locally, thus leading to a decrease in the growth rate. On Earth, these concentration gradients lead to significant buoyancy-driven convection which has been found to be detrimental to crystal growth (Pusey *et al.*, 1988; Nyce & Rosenberger, 1991; Ewing, Forsythe

& Pusey, 1994; Grant & Saville, 1995; Lin, Rosenberger, Alexander & Nadarajah, 1995). These conditions lead to the eventual cessation of growth for protein crystals.

Between nucleation and the 60 h point the crystal shown in Fig. 4, is less than 0.1 mm in size. Based on the previous paragraph it can be expected to grow at a steady rate. The initial rapid increase in the growth rate (Fig. 5) may be attributed to the levelling off of lingering nonuniformities in the solution protein concentration caused by nucleation events. After ~50 h of growth, a steady state is reached, during which time the crystal reaches and exceeds the critical size of 0.1 mm. Beyond this point, as expected, the growth rate decreases due to the
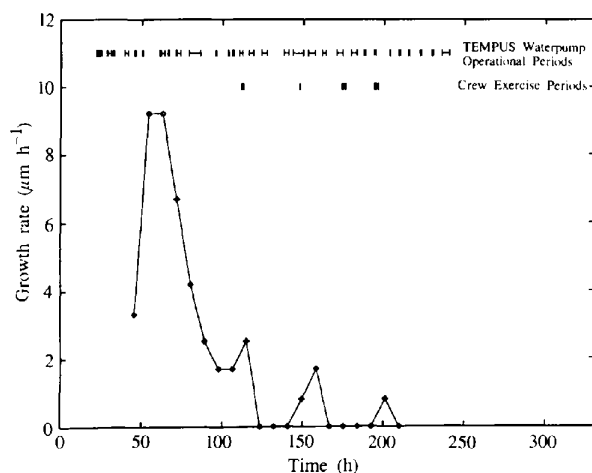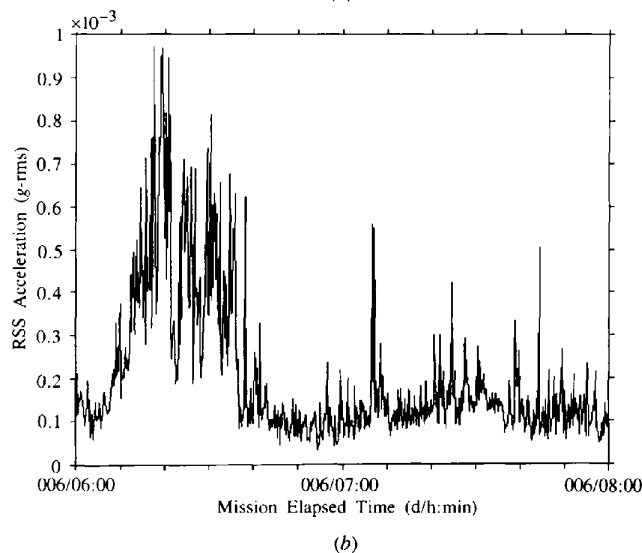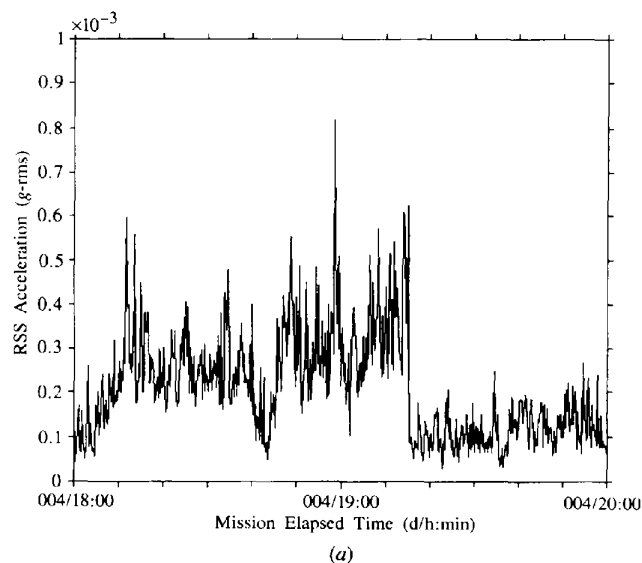

Fig. 6. SAMS plots for the time periods of (a) MET 004/18:00–004/20:00 showing a sample of crew exercise (18:00 to 18:35 and 18:45 to 19:20), (b) MET 006/06:00–006/08:00 again showing crew exercise (06:06 to 06:36).

Fig. 5. Plot of the growth rate over time under microgravity conditions for the crystal depicted in Fig. 6. Accuracy is ±0.5 µm h^{-1} based on pixel size of the images. The time given is in hours after APCF initiation.

formation of concentration gradients around the crystal and the overall depletion of protein in the solution. After 97 h of growth the progressive decline in growth rate towards zero is interrupted by a series of growth spurts. These are clearly correlated with the changes in the acceleration levels in the spacecraft probably due to astronaut activity. The growth rate increases and decreases correspond to the beginning and the end of these activities with a fixed time delay. The concentration does not change significantly until some hundreds of seconds after the event (Ramachandran, Baugher & Naumann, 1995).

Similar time-delayed growth spurts from increased acceleration levels were found in analyses of small-molecule crystal growth systems in microgravity (Nadarajah, Rosenberger & Alexander, 1990; Ramachandran, Baugher & Naumann, 1995). The growth spurts are a result of the increased convection levels which cause protein to be transported from the bulk solution to the crystal surface, increasing the concentration and reducing gradients there. Sustained convection causes a decrease in the growth rate, whilst short convective bursts only cause increased growth rates because of increased protein transport to the crystal (Pusey et al., 1988), as observed here. However, during this time, the protein concentration in the bulk solution continues to be depleted, and each new convection cycle transports less protein than the previous one. This is clearly seen from the progressive decrease in the growth rate peaks after each successive burst of activity in the spacecraft. Eventually the protein concentration in the entire chamber will reach a value too low to drive visible crystal growth and it will be unaffected by any g-jitter.

The SAMS accelerometer heads were mounted in the Spacelab module in the Orbiter payload bay. The APCF experiment was situated in a mid-deck locker, beneath the flight deck, on the Orbiter. The TEMPUS facility itself was mounted in the same rack as the SAMS data-collection head C thus causing signals from TEMPUS to be recorded clearly. A note of caution needs to be sounded because of the difference in location of the accelerometer heads and the APCF experiment. The accelerations recorded by SAMS could be localized disturbances that were not experienced in the mid-deck. Moreover, there could have been localized disturbances in the mid-deck which were not seen in the Spacelab module. There is little data on the transfer of disturbances within the Orbiter. It is quite clear, however, that activity in the flight deck was measured by the SAMS accelerometers in the Spacelab module.

Low-frequency components of g-jitter have a greater influence on particle motion than the high-frequency components. The lower frequencies primarily cause net drift whilst the higher frequencies cause fluctuating movements (Ellison, Ahmadi, Regel & Wilcox, 1995). For small-molecule crystallization experiments these low-frequency components have been shown to have a

greater negative effect (growth rate variation) on the crystal growth (Nadarajah et al., 1990) than the high-frequency accelerations do. The crew exercise generated a maximum recorded g-jitter of about 37 μg for the 2.1–2.5 Hz frequency range, whilst TEMPUS water pump operation generates about 4380 μg in the 79.0–81.0 Hz range. To quantify accurately the localized acceleration environment (those accelerations 'seen' by the APCF), the accelerometer measurements should be made at the crystal growth experiment.

4.2. Orthorhombic crystals

The transition of lysozyme crystals to the orthorhombic form at higher temperatures is well known (Berthou & Jollès, 1974; Cacioppo, Munson & Pusey, 1991). The transition temperature is around 301 K at pH 4.0 and 0.85 M NaCl. However, solubility measurements have clearly indicated that the transition point shifts towards lower temperatures when the pH and NaCl concentration are increased (Cacioppo et al., 1991). At pH 4.5 and 0.51 M NaCl, the transition point is 296 K. At the conditions employed (pH 4.7 and 1.26 M NaCl), the transition point was close to the 293 K operating temperature of the experiment. Small perturbations in the system can cause the formation of the orthorhombic form as observed in the microgravity reactors. Orthorhombic crystals were not observed in the laboratory controls which could be because of slightly different temperatures. The laboratory controls were grown in a polystyrene (insulated) chamber in our home laboratory, which minimized temperature changes, but did not quite have the temperature stability of the APCF (± 0.1 K), perhaps reaching ± 1.0 K. Nevertheless it is a curious observation that not only did the orthorhombic needles occur in the microgravity chamber, but also that one such particularly well formed needle grew directly out of the surface of a tetragonal face (Fig. 1c)

4.3. CCD video operation

The sampling rate for CCD video images in this experiment was limited because the APCF is a multiuser facility. The video system records images from several reactors in turn leading to a rather long time span of approximately 8 h 40 min between successive observations of a single reactor. The video system was configured pre-mission and there is no control over it from the ground. Ideally crystal growth video monitoring should be conducted at small time intervals initially, with less frequent observations occurring as the crystal growth continues. A second limitation was that in this case a narrow field-of-view optics system was used. This choice gave us the high-resolution images of the crystal in Fig. 4 but lost the ability to achieve a statistical sample of data from other crystals within the reactor. Finally, this system records images from one plane of the reactor with a small depth of focus. In future experiments it would be useful

to have two cameras, mounted perpendicular to each other, so that the crystal growth and any movement may be recorded in orthogonal directions.

5. Concluding remarks

We believe the value of CCD video observation as a diagnostic tool for protein crystal growth is well illustrated here, and in another microgravity study under different conditions and using another protein (Chayen, Snell, Helliwell & Zagalsky, 1997). The limitations of current apparatus are also shown and, thus, indicating valuable improvements which can be made for future hardware. The use of accelerometer data as an additional diagnostic tool allows useful correlation between the crystals' growth rates and the microgravity environment. Correlations such as these will provide useful information for future crystal growth experiments conducted in a microgravity environment. The correlation between crystal growth and environment could also be used, with a standard test protein, to assess respective missions in their suitability for protein crystallization and specify an ideal mission profile.

The observation of the spurts and lulls in the growth rate of the tetragonal crystal examined in considerable detail here, may be responsible for the decrease in perfection (albeit still much better than earth grown) when compared with crystals grown on a previous mission (Snell *et al.*, 1995) where only a single crew was used (as compared to the double crew on IML-2) offering periods of low g-jitter during sleeping hours. These variations in growth rate may well be the cause of imperfections or mosaic block structure as evidenced from topographic and X-ray analyses of these crystals in our earlier papers (Chayen *et al.*, 1996; Stojanoff, Siddons, Snell & Helliwell, 1996; Helliwell, Snell & Weisgerber, 1996).
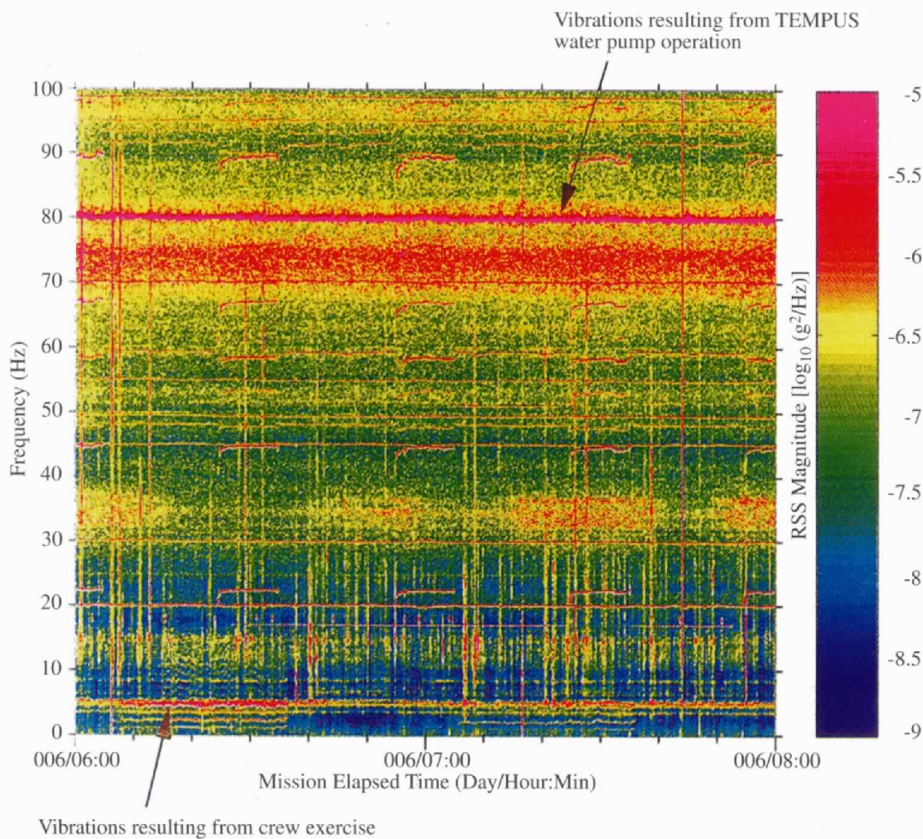
Fig. 7. Spectrogram of SAMS data shows TEMPUS water pump operation seen at 80 Hz throughout and crew exercise seen at 5 Hz from MET 006/06:06 to 006/06:36. These plots are produced by stacking successive time slices of power spectral densities recorded in approximately 16.4 s intervals and assigning a colour to the base 10 logarithm of the PSD intensity. Note that the power spectral density (PSD) magnitude is synonymous with the grms or g-level for a disturbance. To perform such conversion the integral of the PSD over the frequency range of interest must be computed.

References

Ataka, M. & Asai, M. (1988). *J. Cryst. Growth*, **90**, 86–93.

Berthou, J. & Jollès, P. (1974), *Biochim. Biophys. Acta*, **336**, 222–227.

Bosch, R., Lautenschlager, P., Potthast, L. & Stapelmann, J. (1992). *J. Cryst. Growth*, **122**, 310–316.

Cacioppo, E., Munson, S. & Pusey, M. L. (1991). *J. Cryst. Growth*, **110**, 66–71.

Chayen, N. E., Boggon, T. J., Cassetta, A., Deacon, A., Gleichmann, T., Habash, J., Harrop, S. J., Helliwell, J. R., Neih, Y. P., Peterson, M., Raftery, J., Snell, E. H., Haedener, A., Niemann, A. C., Siddons, D. P., Stojanoff, V., Thompson, A.W., Ursby, T. & Wulff, M. (1996). *Q. Rev. Biophys.* **29**(3), 227–278.

Chayen, N. E., Radcliffe, J. W. & Blow, D. M. (1993). *Protein Sci.* **2**, 113–118.

Chayen, N. E., Snell, E. H., Helliwell, J. R. & Zagalsky, P. F. (1997). *J. Cryst. Growth*, **171**, 219–225.

DeLombard, R. & Finley, B. D. (1991). *NASA Technical Memorandum* 105301.

DeLombard, R., Finley, B. D. & Baugher, C. R. (1992). *NASA Technical Memorandum* 105652.

Durbin, S. D. & Feher, G. (1986). *J. Cryst. Growth*, **76**, 583–592.

Ellison, J., Ahmadi, G., Regel, L. & Wilcox, W, (1995). *Microgravity Sci. Technol.* **8**, 140–147.

Ewing, F., Forsythe, E. & Pusey, M. L. (1994). *Acta Cryst.* D**50**, 424–428.

Grant, M. L. & Saville, D. A. (1991). *J. Cryst. Growth*, **108**, 8–18.

Grant, M. L. & Saville, D. A. (1995). *J. Cryst. Growth*, **153**, 42–54.

Helliwell, J. R., Snell, E. H. & Weisgerber, S. (1996). *Proceedings of the European Conference on Microgravity Research, Springer Verlag Lecture Notes in Physics*, edited by L. Ratke, H. Walter & B. Feuerbacher, pp. 155–170. Berlin/Heidelberg: Springer-Verlag.

Howard, S. B., Twigg, P. J., Baird, J. K. & Meehan, E. J. (1988). *J. Cryst. Growth*, **90**, 94–104.

Lin, H., Rosenberger, F., Alexander, J. I. D. & Nadarajah, A. (1995). *J. Cryst. Growth*, **151**, 153–162.

Long, M. M., DeLucas, L. J., Smith, C., Carson, M., Moore, K., Harrington, M. D., Pillion, D. J., Bishop, S. P., Rosenblum, W. M., Naumann, R. J., Chait, A., Prahl, J. & Bugg, C. E. (1994). *Microgravity Sci. Technol.* **7**, 196–202.

Nadarajah, A., Rosenberger, F. & Alexander, J. I. D. (1990). *J. Cryst. Growth*, **104**, 218–232.

Nyce, T. A. & Rosenberger, F. J. (1991). *J. Cryst. Growth*, **110**, 52–59.

Pusey, M. & Naumann, R. (1986). *J. Cryst. Growth*, **76**, 593–599.

Pusey, M. L., Snyder, R. S. & Naumann, R. (1986). *J. Biol. Chem.* **261**, 6524–6529.

Pusey, M., Witherow, W. & Naumann, R. (1988). *J. Cryst. Growth*, **90**, 105–111.

Ramachandran, N., Baugher, Ch. R. & Naumann, R. J. (1995). *Microgravity Sci. Technol.* **7**, 170–179.

Snell, E. H., Helliwell, J. R., Boggon, T. J., Lautenschlager, P. & Potthast, L. (1996). *Acta Cryst.* D**52**, 529–533.

Snell, E. H., Weisgerber, S., Helliwell, J. R., Weckert, E., Hölzer, K. & Schroer, K. (1995). *Acta Cryst.* D**51**, 1099–1102.

Snyder, R. S., Fuhrmann, K. & Walter, H. U. (1991). *J. Cryst. Growth*, **110**, 333–338.

Stojanoff, V., Siddons, D. P., Snell, E. H. & Helliwell, J. R. (1996). *Synchrotron Radiat. News*, **9**(1), 25–26.